2013 American Control Conference (ACC)
Washington, DC, USA, June 17-19, 2013

State Estimation of Fast-Rate Systems using Slow-Rate Image Sensors

Jacopo Tani[1] Sandipan Mishra [1] and John Wen[2]

Abstract— **This paper presents algorithms for state estimation of adaptive optics (AO) systems with fast-rate actuators and slow-rate image sensors. Typically, the information obtained from these slow-rate image sensors is the time-averaged output measurement during the exposure time. The additional information available in the image measurement (in the form of an intensity distribution) is discarded. In order to fully extract information from these blurry measurements, the image sensor is modeled as an integrative intensity sensor. The integrative intensity sensor is a transform from temporal outputs to pixel-domain measurements. Thus, the state estimation problem for the AO system is recast into a multi-rate estimation problem from a non-linear output measurement. Based on this formulation, we propose and compare estimation algorithms that exploit the unique properties of the non-linear integrative sensor model. Experimental results on a fast-rate beam steering mirror and a slow-rate image sensor verify that using the integrative sensor model and exploiting its structure for state estimation can result in lower prediction error.**

I. Introduction

Image sensors are now prevalent as feedback measurement mechanisms for a wide variety of applications. The fundamental limitation of these image sensors is the frame update rate, which is typically much lower than the actuator update rates. The image sensors deliver temporally integrated measurements over the exposure period, which are conventionally interpreted as the *time-average* of the image feature of interest. A typical vision-feedback system is therefore usually a multi-rate system, with a fast-acting actuator and a slow image sensor. There is a rich body of literature on identification, estimation, and control of such multi-rate systems [1]. Lifting techniques, introduced in [2], are powerful analysis and synthesis tools for multi-rate system identification, estimation, and control [3]. Using multi-rate techniques for identification, estimation, and control of image-feedback systems can certainly enhance closed-loop performance [1]. However, loop bandwidth will be still constrained by the fact that the image sensor provides limited information at a slow rate.

In image processing, *motion blur* [4] is observed when an image sensor captures relative motion of an object during the exposure time. Deblurring [5] of a motion-blurred image is an *ill-posed inverse problem* [6]. As an example, the image trace of an object moving left to right will be indistinguishable from that of the object moving right to left. Several algorithms have been proposed for extracting motion from blur [4], with various assumptions that eliminate this ill-posedness (such as assuming a known motion profile, constant velocity, constant acceleration, etc.). While these algorithms are effective for image restoration, they are inadequate for accurate dynamics reconstruction since they focus primarily on determining the deblurred image, not the motion field. Furthermore, they are not implementable in real-time because of computational complexity. These drawbacks, while not relevant for image reconstruction, are of prime importance in estimating dynamics for real-time feedback control.

To address this issue, in [7], the integrative image sensor was modeled as a non-linear transform, i.e., the image sensor transforms temporal information about the motion of the object being imaged into a spatial intensity distribution. This property of the image sensor can be used to *extract output time-history* and hence *reconstruct motion (output dynamics) during the exposure time*. Extraction of time-history at a fast-rate from the slow-rate integrative sensor promises to break the barrier of control bandwidths limited to frame update rates of the image sensor in applications that rely on image sensor feedback. In [7], an extended Kalman filter was used for multi-rate estimation using the first and second moments of the image. While this gives performance enhancement over the simple first moment-estimation schemes used for AO systems, there is still a substantial amount of information unused and discarded from the intensity distribution.

It is clear that information in the intensity distribution can be used to estimate the state more accurately through a suitable inversion of the sensor transform. As mentioned earlier, because of the ill-posed-ness of this inverse problem, some form of regularization is necessary. In this paper, we propose a regularization that uses the *dynamic model of the underlying system* to remove the ill-posed-ness. Therefore, we propose and experimentally validate a multi-rate algorithm that uses a model of the underlying system to estimate the state at the fast actuator rate, from noisy measurements at much slower rates than the observed dynamics. The state estimation is accomplished through the minimization of a predicted image error.

Our motivating application is adaptive optics (AO), which manipulates wavefront by dynamically changing the optical path [8]–[11]. In a typical closed-loop AO configuration (for a telescope), the actuator is a MEMS deformable mirror, capable of operating in the KHz range, and the feedback is provided by a wavefront sensor (e.g., Shack-Hartmann sensor [12]) operating at a much lower rate (e.g., $10-50$ Hz sampling rate for a 30×30 lenslet arrays). The performance limiting component of the wavefront sensor is the image

[1] Jacopo Tani (tanij@rpi.edu) and Sandipan Mishra (mishrs2@rpi.edu) are in the Deparment of Mechanical, Aerospace, and Nuclear Engineering, Rensselaer Polytechnic Institute, Troy, NY, USA

[2]John Wen (wenj@rpi.edu) is in the Department of Electrical, Systems, and Computer Engineering, Rensselaer Polytechnic Institute, NY, USA

sensor array.

In this paper, we will consider the general problem of state estimation of a multi-rate system with a fast rate actuator and a slow rate image sensor. We then pose the multi-rate non-linear estimation problem by using an integrative-sensor model of the camera. To illustrate the approach and experimentally validate our results, we use a setup consisting of a tip-tilt fast steering mirror and a CCD image sensor.

II. Integrative Image Sensor

A. Image Sensor Triggering

The image acquisition process is characterized by the following four timing parameters:

- Acquisition time, T_a. Instant at which the image sensor is triggered for the first time.
- Exposure time, T_e: the length of the actual image acquisition window.
- Readout time, T_r: the time to transfer measured information from the sensor to processor memory.
- Slow sample rate, T_s: the time between two successive exposure windows. Clearly, $T_s \geq T_r + T_e$.

The first two parameters are user-specified. The readout time is usually the bottleneck for the sensor operation.

B. Image Sensor Modeling

We let: $\eta \in \mathscr{N} := \{(\eta_x, \eta_y) | \eta \in [(0,0), (\eta_{x_{\max}}, \eta_{y_{\max}})]\}$, with $\eta \in \Re^2$, parametrize the spatial dimension (pixel domain) $\mathscr{N}$. We define $Y^y(\cdot) \in \mathscr{N}$ to be the output of the image sensor, a 2D intensity map (image), generated by the observed dynamics $y(t)$ which is the output of the system within the exposure time of the image sensor, i.e. $t \in T := [T_a, T_a + T_e]$. $y(\cdot) \in L_2[T]$.

Remark: $y(\cdot)$ here is intended as the system output *as it is seen by the image sensor*, i.e. it is defined on the pixel domain. There will be a function that assigns a spatial domain location to the observed dynamics at every time instant which depends on the positioning of the image sensor relative to the observed system. In the following we neglect this for ease of notation.

We assume $Y^y(\cdot)$ is formed by integrating an image kernel $\Psi(\cdot)$, corresponding to the image $Y^{y\equiv 0}(\cdot)$, over the exposure period T with the acquisition command issued at T_a: $Y^y(\cdot) = \mathscr{C}_\Psi(y) + n(\cdot)$ where $n(\cdot)$ includes the random and shot noise of the image sensor and $\mathscr{C}_\Psi : L_2[T_a, T_a + T_e] \to L_2(\mathscr{N})$ is given by:

$$\mathscr{C}_{\Psi, T_e, T_a}(y) := \int_{T_a}^{T_a + T_e} \Psi(\eta - y(t))\, dt. \tag{1}$$

To simplify notation, we will hereafter include only the all or part of the subscripts of $\mathscr{C}$ and superscripts of Y if necessary. Note that $\Psi(\eta - y(t))$ is simply the image kernel centred at $y(t)$. In the ideal case the image kernel can be assumed to be a point centred at the origin, $\Psi(\cdot) = \delta(\cdot)$. Fig. 1 shows an example of the relationship between the time-domain output $y(\cdot)$ and the pixel domain image $\mathscr{C}_\Psi(\cdot)$.

C. Point Source and Point Spread Function

In the case of point light source, as generated by a focused laser beam or a guide star (as in AO applications), the image kernel, Ψ, is simply the point spread function (PSF). In the ideal case, the image of the point source is also a point and Ψ is then a delta function. In the case of a laser light source, the intensity profile is typically a 2D Gaussian. The optical aberration of a point source may also be approximated by a 2D Gaussian profile. The PSF Ψ is then:

$$\Psi(\eta) = a e^{-\frac{1}{2}(\eta - \eta_0)^T \Sigma^{-1} (\eta - \eta_0)}$$

where η_0 is the center of the Gaussian, a is the height of the peak, and Σ is the 2×2 covariance matrix. The PSF may be obtained experimentally by holding $y(t)$ at zero. The PSF is then approximately $Y(\eta)/T_e$. The effect of noise may be reduced by averaging Y over multiple exposures.

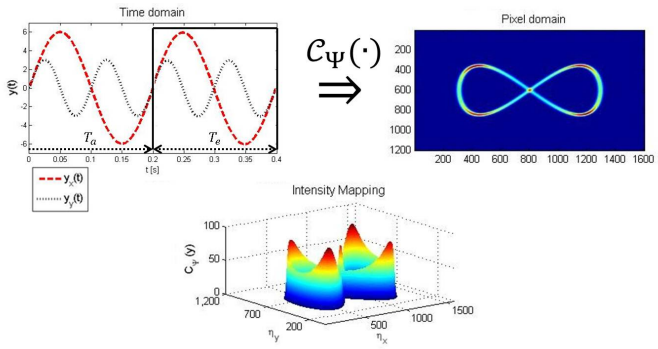

Fig. 1. Top left: time domain signals. Top right: the corresponding 2D pixel domain representation of the image sensor measurement. Bottom: 3D visualization of the intensities.

III. Problem Formulation

Recalling that T_f is the sampling time of the fast system, we define: $N_e := T_e/T_f$ to be the number of (fast) time instants **in an exposure window** and $N := T_s/T_f$ to be the number of time instants **in a slow step**, i.e. the time between successive outputs from the image sensor (Sec. II-A). Both N,N_e are positive integers and clearly $N_e < N$. Based on the image sensor model and on the fast-rate actuator model:

$$\begin{aligned} x_f(k+1) &= A_f x_f(k) + B_f u_f(k) + B_w w_f(k) \\ y_f(k) &= C_f x_f(k) + D_f u_f(k) \end{aligned} \tag{F.S.}$$

we pose the following *state estimation problem* for systems with a fast-rate mirror and a slow integrative measurement. The output y_f is not directly measured; instead it is to be inferred from the j^{th} slow-rate integrative sensor output, Y_j, obtained at a rate T_s:

$$Y_j(\cdot) = \mathscr{C}_{jT_s}(y_j)(\cdot) + n_j(\cdot), \quad j = 0, 1, \ldots$$

where $y_j = y_f(jN + l) \quad l \in \{1, 2, \ldots N_e\}$, i.e. the output of the fast system within the j^{th} exposure window, e.g. the signal within the exposure window in the top left picture in fig. 1. The general estimation problem posed in this paper is to estimate $x_f(k)$ by using $\{Y_j\}_{j=0}^J$, for some $J = \left\lfloor \frac{k}{N} \right\rfloor$.

IV. State Estimation

In this section we introduce the moments of an intensity distribution $\mathscr{C}_\Psi$ generated by a non ideal image kernel $\Psi(\cdot)$. We then proceed to define three observers which

performances will be then compared in the experimental results section V-A. The first observer **(O1)** will apply its correction based on the center of gravity (first moment) of the measured intensity distribution; the second one **(O2)** will use the first and second moments while the last one **(O3)** will use information from the whole intensity distribution measurement.

Moments of the Intensity Distribution

Moment computations of intensity distributions have been used frequently in image deblurring algorithms [4], [13]. The p^{th} moment of the univariate intensity distribution $Y(\cdot) \in \mathscr{N}$ is defined as:

$$y^{(p)} = \frac{\int_{-\infty}^{\infty} \eta^p Y(\eta) d\eta}{\int_{-\infty}^{\infty} Y(\eta) d\eta}.$$

For $\Psi(\cdot) = \delta(\cdot)$, this higher order moment reduces to:

$$y_{\delta}^{(p)} = \frac{1}{T_e} \int_{\tau=T_a}^{T_a+T_e} y^p(\tau) d\tau. \tag{2}$$

Therefore, for this special case, higher spatial moments of the intensity distribution are time-averages of *powers of the output* within the exposure window (y_f^p). The p^{th} moment of $\mathscr{C}_{\Psi}$ can be expressed as the power of a binomial where the moments are intended in place of the powers, i.e.:

$$y_{\mathscr{C}}^{(p)} = \sum_{i=0}^{p} \binom{p}{i} y_{\Psi}^{(p-i)} y_{\delta}^{(i)} \tag{3}$$

where the $y_{\Psi}^{(p)}$ moments are given by:

$$y_{\Psi}^{(p)} = \frac{\int_{\Re^2} \eta^p \Psi(\eta) d\eta}{\int_{\Re^2} \Psi(\eta) d\eta}$$

and the $y_{\delta}^{(p)}$ moments are given by eq. (2). E.g. the first (or *center of gravity* of the image y_{CG}) and second moments can be written (hereafter neglecting the subscript $\mathscr{C}$) as:

$$y_{CG} := y^{(1)} = y_{\Psi}^{(1)} + y_{\delta}^{(1)} = \eta_0 + \frac{1}{T_e} \int_{T_a}^{T_a+T_e} y_f(\tau) d\tau$$
$$y^{(2)} = y_{\Psi}^{(2)} + 2 y_{\Psi}^{(1)} y_{\delta}^{(1)} + y_{\delta}^{(2)}.$$

Since the estimation and control algorithms are designed in discrete time, we may approximate the moment equation, eq. (3) as a finite sum with a sampling time T_f (we are assuming here that acquisition time T_a is zero). Recalling (sec. II-C) that η_0 is the pixel where the $\Psi(\cdot)$ is centred (e.g. where the peak of the Gaussian is located):

$$y^{(p)}(j) = \sum_{i=0}^{p} \binom{p}{i} \frac{\sum_{r=0}^{\eta_{xmax}} (r-\eta_0)^{p-i} \Psi(r)}{\sum_{s=0}^{\eta_{xmax}} \Psi(s)} \cdot \frac{1}{N_e} \sum_{m=0}^{N_e-1} (y_f(jN+m))^i. \tag{4}$$

It is key to note that the spatial moments are projections of the intensity profile onto the polynomial basis set $\mathscr{B} = \{b_n : b_n(\eta) = \eta^n, n \in Z^+\}$. Alternative basis functions may be designed to improve computational tractability based on the image feature of interest (i.e. the image kernel) and/or the nature of information to be extracted. In the following section, we present state estimation schemes for systems with integrative intensity sensor measurements, for the univariate intensity distribution case. The case of a 2D intensity sensor grid can be developed from a direct extension of these results.

***(O1)** Discrete-time Linear Estimation*

We first present the standard multi-rate estimation scheme that uses only the first moment (time averaged output over the exposure time). This is the typical state of the art for AO systems with a slow-rate measurement.

Since the first moment is the averaged value of the output (y_f) of the fast-rate system during the exposure time, we have the following lifted multi-rate system description when we use the first moment (eq. (4), $p = 1$) as the only output measurement ($y_m^{(1)}(\cdot)$):

$$\begin{aligned} x_s(j+1) &= A_s x_s(j) + B_s u_s(j) + B_{w,s} w_s(j) \\ y_m^{(1)}(j) &= C_s x_s(j) + D_s u_s(j) + n_1(j) \\ w &\sim \mathscr{N}(0, W) \end{aligned} \tag{S.S.}$$

where the process noise is w and the measurement noise in the moment is n_1. We use the subscript s to stress that this system is expressed in the slow time rate T_s, it is therefore the slow system (S.S.) as opposed to the fast system (F.S.). In [7], the dependence of the measurement noise on the camera noise is explicitly derived.

In the above slow system:

$$\begin{aligned} A_s &= A_f^N \\ B_s &= \begin{bmatrix} A_f^{N-1} B_f & A_f^{N-2} B_f & \dots & B_f \end{bmatrix} \\ C_s &= \begin{bmatrix} C_f + C_f A_f + \dots + C_f A_f^{N_e-1} \end{bmatrix} \\ \bar{D}_s &= \begin{bmatrix} \sum_{i=0}^{N_e-1} C_f A_f^i B_f & \sum_{i=0}^{N_e-2} C_f A_f^i B_f & \dots & C_f B_f \end{bmatrix} \\ D_s &= \begin{bmatrix} \bar{D}_s & 0 \end{bmatrix}, \end{aligned}$$

where the 0 in D_s is a vector of appropriate dimensions to match the length of $u_s(j)$, which is the stacked vector of fast inputs within the j^{th} slow step, i.e.:

$$u_s(j) = [u_f((j-1)N+1) \; u_f((j-1)N+2) \; \dots \; u_f(jN)]^T \tag{5}$$

Similarly $B_{w,s} w_s(\cdot)$ is just the stacked version of $B_w w_f(\cdot)$ as in (5). It is easy to show that (A_s, C_s) is an observable pair if (A_f, C_f) is observable. Thus, a standard Luenberger observer can be designed for the multi-rate system by placing the poles of $(A_s - LC_s)$ as below:

$$\hat{x}_s(j+1) = A_s \hat{x}_s(j) + B_s u_s(j) + L\left(y_m^{(1)}(j) - \hat{y}^{(1)}(j)\right)$$

where by $\hat{y}^{(p)}(j)$ we represent the predicted moment according to (4) (here with $p = 1$).

(O2) *Using Higher Moments for Estimation*

Using the center of mass of the intensity distribution only utilizes a fraction of the information available in the sensor measurement. For example, by using the second moment of the intensity distribution, we have an additional output equation:

$$y_m^{(2)}(j) = h(x_s(j)) + n_2(j)$$

where $h(x_s(j))$ is (4) with $(p=2)$. Thus, we now have a nonlinear output $(y_m^{(2)})$ in addition to the linear output $(y_m^{(1)})$. In [7], an extended Kalman filter was designed based on the first and second moments of the intensity measurement. Following a similar procedure to obtain the time-varying observer gains $L_p(j)$, higher moments of the intensity distribution, $y^{(p)}$ may be used as additional output for better state estimation.

$$\hat{x}_s(j+1) = A_s\hat{x}_s(j) + B_s u_s(j) + \begin{bmatrix} L(j) \\ L_2(j) \\ \cdots \\ L_p(j) \end{bmatrix}^T \begin{bmatrix} y_m^{(1)}(j) - \hat{y}^{(1)}(j) \\ y_m^{(2)}(j) - \hat{y}^{(2)}(j) \\ \cdots \\ y_m^{(p)}(j) - \hat{y}^{(p)}(j) \end{bmatrix}$$

(O3) *Using Image Prediction Error for Estimation*

In the most general case of an intensity distribution, it is logical to use the *entire* intensity profile for obtaining the best possible state estimate instead of spatial moments. We now present an estimation algorithm that uses the error between the measured and predicted intensity profiles, i.e., $(Y_j(\cdot) - \mathscr{C}(\hat{y}_j))$ to drive the estimation of the state. Note that $Y_j(\cdot)$ is the measured image at the j^{th} slow step and $\mathscr{C}(\hat{y}_j)$ is the predicted image using the estimated state $\hat{x}_s(j)$.

Thus, we have the following two-stage state estimation scheme. First, the best guess of the state $x_s(j)$ is obtained by solving the optimization problem below:

$$\hat{x}^{opt}(j) = \arg\min_{\hat{x}_s(j)\in\Re^n} \left\| Y_j(\cdot) - \mathscr{C}(\hat{y}_j) \right\|^2$$

$$\text{subject to } \hat{y}_j(i) = C_f A_f^i \hat{x}_s(j) + \sum_{n=0}^{i-1} C_f A_f^{i-n-1} B_f u_{s,j}(n)$$

$$i = \{0, 1, \cdots N_e - 1\}$$

Where $u_{s,j}(i)$ is the i^{th} component of the $u_s(j)$ vector defined in (5) and $\|\cdot\|$ is an appropriate norm. Then, this state estimate is propagated forward (open loop) to the next slow step as $\hat{x}_s(j+1) = A_s\hat{x}^{opt}(j) + B_s u_s(j)$.

V. Experimental Apparatus

To validate the proposed algorithm we use the experimental setup shown in Fig. 2(a). A laser source is bounced off a fast steering mirror (FSM) with the resulting image captured by a CCD camera, as represented in Fig. 2(b). The mirror is also equipped with a high bandwidth position sensing diode (PSD) allowing the comparison between the image based technique in this paper with a high quality reference of one of the system states (the output $y_{meas} = x_{f,2}$). The components of the system are described below.

- A two-degree-of-freedom (tip-tilt) *FSM* is used as the plant, (F.S.) which states we intend to estimate. It is driven by piezoelectric actuators and the position is measured by PSD sensors. The mirror is connected to an xPC Target real-time control computer with analog PID closed loop control. The inputs to the system is the commanded angular deflection in the x direction and the output is the actual angular position. The PSD measurements serve as high quality reference for the image based estimation.
- *Focused Laser Beam* passes through a beam splitter, reflects off the FSM surface which deflects it onto the image sensor. Mirror motion causes the laser beam to move on the image sensor plane. The laser has been kept at constant (minimum) power throughout the experiment.
- *CCD Camera* records the light intensity of the laser beam deflecting off the mirror surface.
- *Beam Splitter* deflects the steady laser beam onto the mirror.

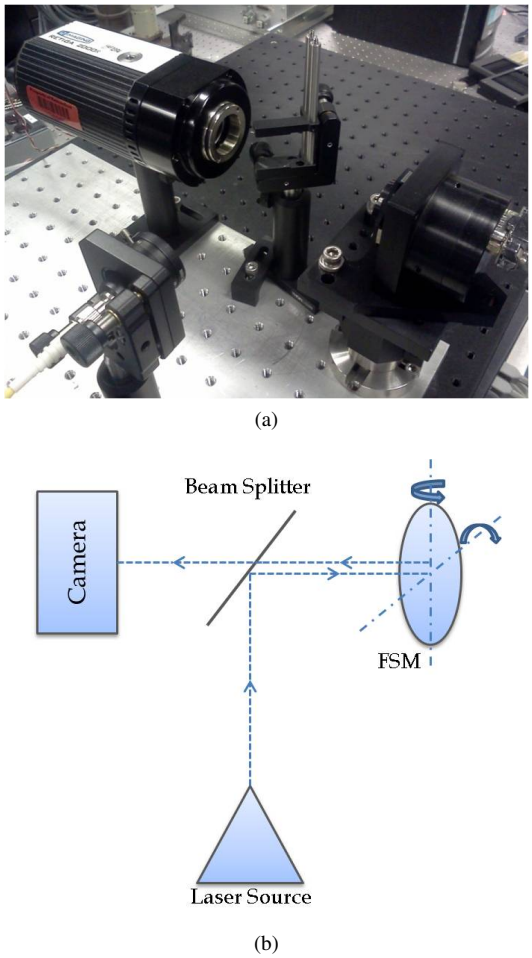

(a)

(b)

Fig. 2. Experimental apparatus (a) showing a CCD camera, a laser source (bottom left), a steerable mirror (right) and a beam splitter. The PSD sensor is built in the CCD camera. (b) A schematic representation of the above.

Observer Design Scenarios

We compare three design scenarios: **(O1)** a Luenberger observer designed based on the lifted system A_s, B_s and pole placement, using *only* the first moment $(y^{(1)})$ of the

intensity distribution as developed in section (V-O1); **(O2)** a Luenberger observer design based on the lifted system A_s, B_s using *both* the first and second moment $(y^{(1)}, y^{(2)})$ of the intensity distribution as developed in section (V-O2) and **(V-O3)** a state-predictor based on the minimization of the infinity-norm of the *image prediction error*, as developed in section (O3). Figure 3 shows a qualitative representation of how the three estimators see the image sensor measurement, i.e. what information of it they use to apply the estimate correction.

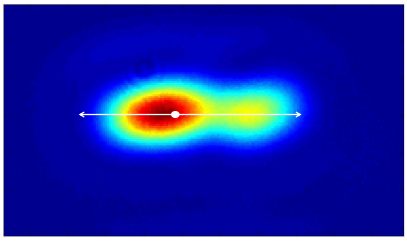

Fig. 3. Qualitative representation of first (circle) and second (line) moments on a measured image. (O1) uses only the first moment to correct its estimate, (O2) uses first and second, (O3) the whole image.

The FSM system has the model $G(j\omega) = G_0(j\omega)(I + W_t(j\omega))$, where:

$$G_0(j\omega) \sim \left[\begin{array}{cc} A_f & B_f \\ C_f & D_f \end{array}\right]$$

with:

$$A_f = \left[\begin{array}{cc} 0 & -1156 \\ 1 & -13.6 \end{array}\right], B_f = \left[\begin{array}{c} 1156 \\ 0 \end{array}\right]$$
$$C_f = \left[\begin{array}{cc} 0 & 1 \end{array}\right], \qquad D_f = 0$$

and the uncertainty $W_t(j\omega)$ has magnitude between $\pm$7dB.

A. Results

The time parameters were set to: $T_f = 1ms$, $T_e = 100ms$, $T_r = 350ms$ and $T_a = 90ms$. The experiment was run for $j = 35$ slow steps (total time of 15.84s). Note that the images are available every $N = 450$ fast-rate steps, therefore the state estimation update is done every 450ms and forward propagated between slow-rate steps according to the the model $G_0(j\omega)$ of the system driven by the input $u_f(\cdot)$. In all cases the estimators are initialized with identical random initial states. Figure 4 shows an overview of the evolution of the output $(\hat{y}_{(\cdot)}(t) = \hat{x}_{f,2})$ of the fast evolving system in the three considered case (O1-3). Only the first few seconds of experiment results are shown for ease of representation. The estimates in the three cases introduced above are compared to the *true* output of the FSM (y_{PSD}) obtained by built in PSD sensors. The image sensor activation pulse is shown as well to highlight the exposure windows and readout times. Figure 5 shows a detail of the output and estimates within a slow-step, i.e. the time interval between successive output measurements. The estimation correction occurs at the end of every slow-step. Figure 6 shows the evolution of the norm of the estimation error at the correction instants $jNT_f + T_a$, i.e. $\varepsilon_{(\cdot)}(j) = \|x_{s,2}(j) - \hat{x}_{s,2}(j)\|$. We show comparisons of

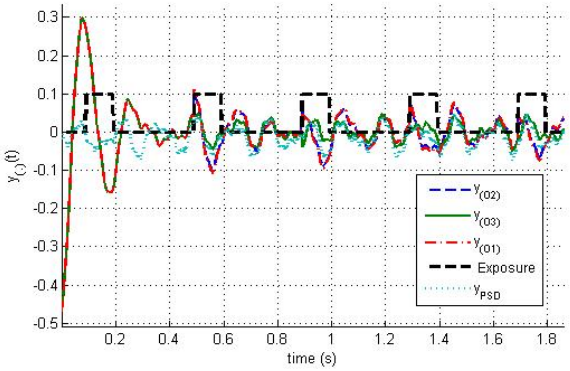

Fig. 4. Overview of the output $y_{(\cdot)}(t) = x_{f,2}$ of the system. The Luenberger estimator (O1), the EKF estimator (O2) and the image prediction based one (O3) are compared with the "true" output of the system (y_{PSD}) as measured by FSM built in PSD sensors.

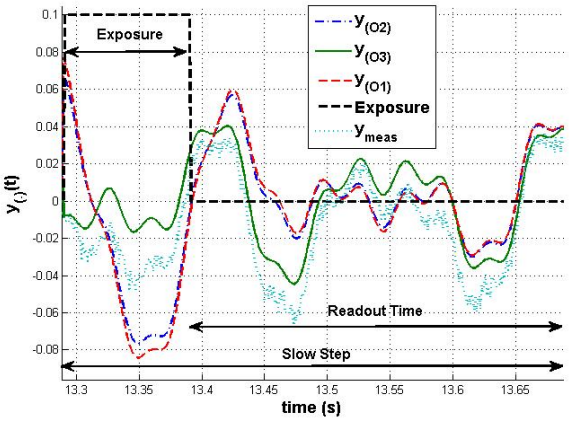

Fig. 5. Detail of the estimation within a slow-step. The correction occurs at the end of the readout time based on the information gathered during the previous exposure window.

only the $x_{f,2}$ because we do not have direct measurements of $x_{f,1}$ to use for validation. Finally fig. 7 shows the evolution of the 2-norm of the estimation error $\|\hat{y}_{(\cdot)} - y_{PSD}(j)\|_2$ for the state variable $x_{f,2} = y_f$. The second order estimator (O2) consistently performs better than the first order one (O1) that uses only the center of gravity of the image, experimentally validating the numerical results presented in [7]. It is moreover evident from the above results that exploiting the dynamic information encoded in the blur of the *whole image* delivers more information rather than considering one or two of its moments. The steady state estimation error mean of (O1) ($\sim$0.59) is bigger than the (O2) estimator ($\sim$0.54) and much bigger than the image-predictor based estimator (O3) ($\sim$0.34), although all cases deliver significant tracking errors. These errors are due to the uncertain model of the system adopted to design the estimators as well as to the process and measurement noises.

VI. Conclusions and Future Work

A model was developed for the class of integrative intensity sensors. The integrative intensity sensor is effectively

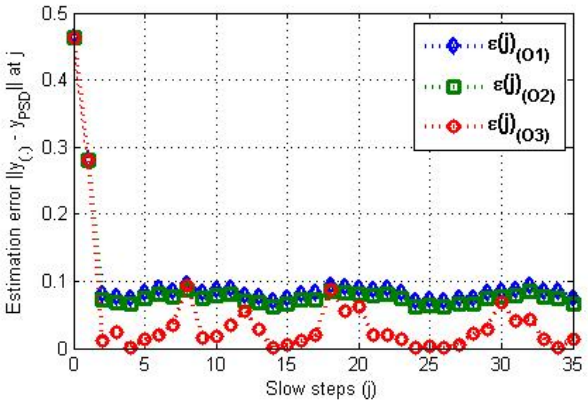

Fig. 6. Norm of the estimation error evaluated at the correction instants, i.e. $\|y_{(\cdot)}(jN) - y_{PSD}(jN)\|$.

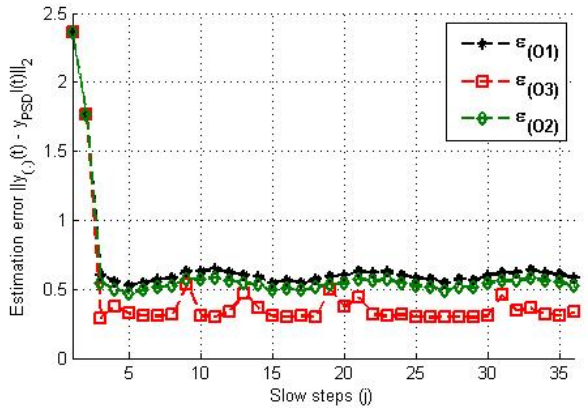

Fig. 7. Two norm of the estimation error evaluated within slow steps, i.e. $\sum_{l=1}^{N_e} \|y_{(\cdot)}(jN+l) - y_{PSD}(jN+l)\|_2$.

a non-linear integral transform from time-domain evolution of the output to a pixel-domain intensity distribution that captures the relative length of time for which the output resides at a given value. Thus, dynamic information (about the output) encoded in the image blur can be extrapolated in the form of moments of the intensity distribution or by directly considering the whole intensity distribution measurement. This information can be used to estimate the states of a fast rate system through slow rate image sensor measurements.

A multi rate estimation algorithm was proposed that estimates the fast evolving state by minimizing the infinity norm of the estimation error in the form of difference of measured and predicted intensity distributions. The measurements are available at a slow rate, when the estimation correction is applied. The states are then open loop propagated until the new measurement is available according to a model of the underlying fast system.

The state estimate obtained through this algorithm was validated on a simplified active optics experimental setup and the results compared to two different Luenberger observers, one using only the first and the other both first and second moments of the intensity distributions. It was shown that the proposed image prediction algorithm outperforms the moments-based estimators both in terms of estimation error at the update instants and in terms of two norm of the tracking error over successive updates.

Several future avenues of research exist for fully exploiting the integrative nature of the image sensor. A theoretical framework to describe the influence of the problem parameters (e.g. the amplitude of the input, the magnitude and nature of the noises, the amount of modeling uncertainty) on the quality of the state estimate must be developed. Moreover the existence of a null space in the inversion of the image sensor transformation leads to the existence of alias solutions. We intend to investigate these issues and propose methods to effectively mitigate them.

ACKNOWLEDGMENT

This work was supported primarily by the National Science Foundation (NSF) through CMMI-1130231, and partially by the NSF Smart Lighting Engineering Research Center (EEC-0812056) and the Center for Automation Technologies and Systems (CATS) under a block grant from the New York State Empire State Development Division of Science, Technology and Innovation (NYSTAR).

REFERENCES

[1] D. Glasson, "Development and applications of multirate digital control," *Control Systems Magazine, IEEE*, vol. 3, no. 4, pp. 2 – 8, 1983.

[2] P. Khargonekar, K. Poolla, and A. Tannenbaum, "Robust control of linear time-invariant plants using periodic compensation," *Automatic Control, IEEE Transactions on*, vol. 30, no. 11, pp. 1088 – 1096, 1985.

[3] J. Wang, T. Chen, and B. Huang, "Multirate sampled-data systems: computing fast-rate models," *Journal of Process Control*, vol. 14, no. 1, pp. 79 – 88, 2004.

[4] W.-G. Chen, N. Nandhakumar, and W. N. Martin, "Image motion estimation from motion smear-a new computational model," *Pattern Analysis and Machine Intelligence, IEEE Transactions on*, vol. 18, pp. 412–425, 1996.

[5] S. Hammett, "Motion blur and motion sharpening in the human visual system," *Vision Research*, vol. 37, no. 18, pp. 2505 – 2510, 1997.

[6] J. Biemond, R. Lagendijk, and R. Mersereau, "Iterative methods for image deblurring," *Proceedings of the IEEE*, vol. 78, no. 5, pp. 856 –883, May 1990.

[7] S. Mishra and J. Wen, "Extracting dynamics from blur," *50th IEEE Conference on Decision and Control and European Control Conference*, Dec. 2011.

[8] H. W. Babcock, "The possibility of compensating astronimical seeing," *Astronomical society of the pacific*, vol. 65, no. 386, pp. 229–236, 1952.

[9] R. K. Tyson and D. E. Canning, "Bit-error rate improvement of a laser communication system with low-order adaptive optics," in *Proc. SPIE, Free-Space Laser Communication and Laser Imaging II,*, 2002, pp. 82–87.

[10] S. P. Poland, D. Burns, W. Lubeigt, B. A. Patterson, G. Valentine, A. J. Wright, and J. M. Girkin, "Use of optimisation algorithmic techniques with active optics for aberration correction in optical sectioning microscopy," W. Jiang, Ed., vol. 6018, no. 1. SPIE, 2005, p. 60181H. [Online]. Available: http://link.aip.org/link/?PSI/6018/60181H/1

[11] J. M. Girkin and P. N. Marsh, "Use of adaptive optics for improved multiphoton imaging," A. Periasamy and P. T. C. So, Eds., vol. 5323, no. 1. SPIE, 2004, pp. 260–266. [Online]. Available: http://link.aip.org/link/?PSI/5323/260/1

[12] B. C. Platt and R. Shack, "History and principles of shack-hartmann wavefront sensing." *Journal of Refractive Surgery*, vol. 17, no. 5, pp. 573–577, 2001.

[13] Y. Zhang, C. Wen, and Y. Zhang, "Estimation of motion parameters from blurred images," *Pattern Recognition Letters*, vol. 21, no. 5, pp. 425 – 433, 2000.